Emergence of synchronization in multiplex networks of mobile Rössler oscillators

Soumen Majhi,[1] Dibakar Ghosh,[1] and Jürgen Kurths[2,3]
[1]*Physics and Applied Mathematics Unit, Indian Statistical Institute, 203 B. T. Road, Kolkata-700108, India*
[2]*Potsdam Institute for Climate Impact Research, Potsdam 14473, Germany*
[3]*Saratov State University, Saratov, Russia*

(Received 28 November 2017; revised manuscript received 1 June 2018; published 4 January 2019)

Different aspects of synchronization emerging in networks of coupled oscillators have been examined prominently in the last decades. Nevertheless, little attention has been paid on the emergence of this imperative collective phenomenon in networks displaying temporal changes in the connectivity patterns. However, there are numerous practical examples where interactions are present only at certain points of time owing to physical proximity. In this work, we concentrate on exploring the emergence of interlayer and intralayer synchronization states in a multiplex dynamical network comprising of layers having mobile nodes performing two-dimensional lattice random walk. We thoroughly illustrate the impacts of the network parameters, in particular, the vision range ϕ and the step size u together with the inter- and intralayer coupling strengths ϵ and k on these synchronous states arising in coupled Rössler systems. The presented numerical results are very well validated by analytically derived necessary conditions for the emergence and stability of the synchronous states. Furthermore, the robustness of the states of synchrony is studied under both structural and dynamical perturbations. We find interesting results on interlayer synchronization for a continuous removal of the interlayer links as well as for progressively created static nodes. We demonstrate that the mobility parameters responsible for intralayer movement of the nodes can retrieve interlayer synchrony under such structural perturbations. For further analysis of survivability of interlayer synchrony against dynamical perturbations, we proceed through the investigation of single-node basin stability, where again the intralayer mobility properties have noticeable impacts. We also discuss the scenarios related mainly to effects of the mobility parameters in cases of varying lattice size and percolation of the whole network.

DOI: 10.1103/PhysRevE.99.012308

I. INTRODUCTION

Complex network theory has offered a valuable platform for the study of emergent collective behaviors, particularly based on the coaction in the interactional topology and coupled dynamical units. Among the diverse emerging asymptotic states, the developing phenomenon of *synchronization* [1,2] has been in the center of research over the past two decades. Synchronization refers to a mechanism in which interacting systems adjust their rhythm over time to achieve a coherent behavior. Synchronization processes are omnipresent in nature and play a crucial role in many different contexts as biology, ecology, climatology, sociology, technology, etc. [1–4].

But notably, most of the previous works dealt with situations where the links between the local dynamical units are presumed to be persistent for all the course of time. However, this sort of simplified assumption may not resemble many practical situations. Indeed, there exists various examples of networks in real-world encircling time evolving interaction structure, where the links associating the nodes vary over time. Networks with time-varying topology [5] may arise in physical systems [6], biological systems [7], communication networks [8–11], social networks [12], modeling of spread of epidemics [13–15], to name only a few. This implies that a shift from the static assumption to dynamical evolution of a network itself is essential for further understanding. In recent times, the study of synchronization in time-varying networks has secured growing attention, particularly, in networks where variation in interaction arises due to mobility in the nodes. In fact, studies have revealed that there are enormous practical evidences in which order emerges among a large number of movable individuals that can interact with each other strictly depending on their proximity. Coordination arising in an ensemble of mobile robots or vehicles was proposed as a procedure of controlling them [16,17]. A transition from disorder to spontaneous order in moving swarming desert locusts was explored by Buhl *et al.* [18]. Uriu *et al.* [19] discussed the issue of cell movement involved in local intercellular signaling which is highly important for morphogenesis during animal development. Particularly, influence of collective cell movement in enhancing synchronization of locally coupled genetic oscillators, explaining synchrony of the segmentation clock in zebrafish somitogenesis was also illustrated [20]. Synchrony among mobile agents is also crucial in several other developments, such as the process of chemotaxis [21], mechanisms in wireless sensor networks, MANET (Mobile Ad Hoc Network), etc. [22,23].

These bring the essentiality of the study of synchronization in dynamical networks of mobile nodes. Regarding this, there exists few works in the literature, e.g., the study in [14] particularly focused on the spread of infectious disease while considering a network of movable oscillators. Ensemble of mobile Kuramoto phase oscillators and chaotic systems

are dealt with in Refs. [24,25] and [26,27], respectively, to analyze the emergence of synchrony. Synchrony in a dynamical network of nodes each associated with integrate-and-fire oscillators communicating with immediate neighbors upon firing time, was elaborately discussed in Ref. [28]. The impacts of noise [29,30], a typical restricted interaction [31] on the collective global synchronous behavior have also been investigated. Other notable works include studies about the effect of self-propulsion on synchrony in mobile oscillators' network [32,33].

We would now like to emphasize that recent research also corroborated that the functionalities arising in one network may awfully influence other networks and, particularly, a node in one network is quite likely a part of another network as well. From social [34] and biological systems [35] to physical and transportation systems [36], it is clear that such interrelationships exist from different contexts. This proves multilayer (multiplex) architecture of networks [37–46] to be quite effective in describing many systems. This also suggests that the study of dynamical evolution processes on top of multilayer networks, which differ from those on its monolayer counter parts [47], are the next frontier in network theory research. In this context, one must also note that there are several other processes, such as epidemic spreading which are best captured by networks exhibiting multiplex structure [48,49]. Among several dynamical states, the existence of explosive synchronization [50], breathing synchronization [51], cluster synchrony [52], inter- and intralayer synchronization [53–57], chimera states [58–60] in such interdependent networks has been demonstrated earlier.

Nevertheless, to the best of our knowledge, all previous studies have contemplated with either completely time-static (or space static) networks with multilayer (multiplex) formalism or networks of spatially moving nodes over a single layer. But, rigid connections between individuals for modeling several interdependent processes, are less practical. Rather mechanisms following which interactions between particulars evolve over time relying on the physical proximity among the individuals, must be employed. In fact, the extremely crucial dynamical consequences arising in a multiplex network of mobile nodes, is yet to be given its due attention. For instance, public transport networks serve as a paradigmatic example of time-varying (spatial) multilayer networks [61]. Multilayer (multiplex) also presents a natural framework for analyzing ecological systems [62] as it allows one to explore influences due to interlayer and intralayer interactions, where mobility of the species can play decisive role to bring self-organization [63,64]. Moreover, the inclusion of space and networks of mobile individuals clearly appears to be very much relevant in the study of epidemic spreading. Indeed, infectious diseases spread as the individuals travel and interact. Particularly, spreading processes through multiple routes of transmission [48] can be explored best in spatial multiplex formalism [65,66].

So, the present article deals with a quite realistic formalism of networks while following a two-layer multiplex formation in which nodes in each layer are allowed to move performing a two-dimensional (2D) lattice random walk and consequently interactions among the entities change over time due to that spatial movement. The interlayer links connecting the replicas, here, are the representatives of the interdependencies of the layers within the network that describe how a given node in one layer and its counterpart in another layer (i.e., the replicas) influence each other. Owing to this network framework, there are two types of interaction strengths, the interlayer strength ϵ and intralayer strengths k_1 and k_2, together with the mobility parameters, such as the vision ranges ϕ_1, ϕ_2 and step sizes u_1, u_2 (a detailed description of them are given later). With variations of these network parameters, we witness inter- and intralayer synchronization states in coupled Rössler dynamical systems. We present an analytical study on the necessary conditions for the emergence and stability of such synchronization states that excellently match the numerically obtained results. We thoroughly analyze the persistence of interlayer synchrony against both topological (like link based attack in the form of progressive demultiplexing and also in response to layer node based attacks in terms of successively made static nodes)and dynamical (in terms of single-node basin stability) perturbations. The effects of intralayer mobility parameters in enhancing robustness of interlayer synchronization under both topological and dynamical disturbances are explained. In this context, we would like to emphasize that in most of the earlier works on synchronization, completely percolated single-component networks are mainly dealt with. But the intermittent connectivity pattern in our work does not necessarily always lead to a single-component network. So as far as the impacts of the mobility parameters are concerned, we relate the incarnation of synchronous states to the evolution of giant connected component in the network [67].

The present work is organized as follows: Sec. II is devoted to the description of the movement algorithm of the layer nodes, whereas Sec. III deals with the formulation of the proposed dynamical network model. The appearance of inter- and intralayer synchrony as a result of variation in different network parameters is discussed in Sec. IV with subsections A, B, and C, respectively, devoted to numerical results, linear stability analysis, and discussions on effects of vision range and step size. In Secs. V A and V B, respectively, we illustrate the survivability of interlayer synchronous state against so-called structural attacks. Dynamical perturbations to the synchronization manifold are explained in Sec. VI. We further discuss the possibility in enhancing the robustness of the synchronized state via variation in the mobility parameters in both Secs. V and VI. Finally, in Sec. VII, we provide concluding remarks on the obtained results.

II. MOBILITY IN THE LAYER NODES

This section deals with the explanation of the mechanism through which the nodes in two layers move in a finite region of the two-dimensional (2D) space. To start with, in each of the layers, we randomly place N nodes in a $P \times Q$ node mesh, while associating a position coordinate (ξ_i^k, η_i^k) for the ith node of kth layer, $i = 1, 2, \ldots, N$ and $k = 1, 2$. The movement scheme, we undertake, basically follows a 2D-lattice random walk algorithm, which is a generalization of the well-known 1D-lattice random walk on the integer line [68]. A simple change in the position coordinates (ξ_i^k, η_i^k) for the ith node after each (and every) time iteration to make the

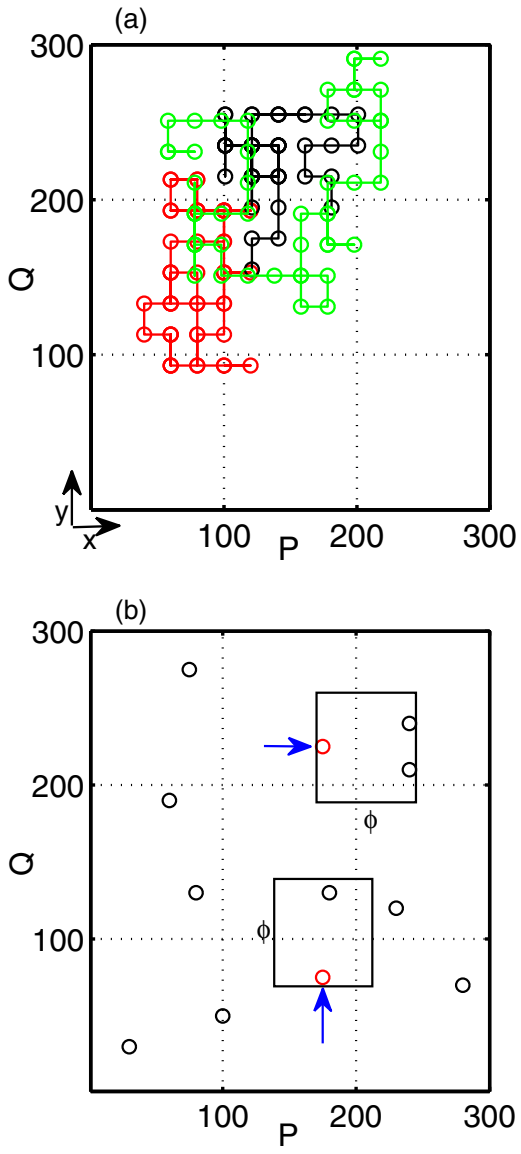

FIG. 1. (a) Typical random walk movements of three particular nodes (denoted by circles) starting from random positions with step size $u = 20$ over a finite time interval in a $P \times Q$ two-dimensional grid where $P = Q = 300$. (b) The interactional picture at a particular instant of time with a view of the vision sizes (having area ϕ^2) for particularly two nodes (red circles) moving towards positive x and positive y directions (blue arrows). For clarity of the figures, only a few moving nodes in a single layer are shown for each case.

nodes to move either to right or left and to up or down [cf. Fig. 1(a)] with step size u_k, is applied in the following way:

(a) The movements along the positive x axis (the right) or positive y axis (the up) or along the negative x axis (the left) or negative y axis (the down) directions are defined as

$$\xi_i^k(\tilde{t} + \delta\tilde{t}) = \xi_i^k(\tilde{t}) + u_k \cos\theta_i^k,$$
$$\eta_i^k(\tilde{t} + \delta\tilde{t}) = \eta_i^k(\tilde{t}) + u_k \sin\theta_i^k, \quad (1)$$

corresponding to the randomly chosen $\theta_i^k \in \{0, \frac{\pi}{2}, \pi, \frac{3\pi}{2}\}$. Here $\delta\tilde{t}$ is the characteristic time scale for the movement of the nodes.

(b) For the next time iteration with a new set of random numbers θ_i^k for $i = 1, 2, \ldots, N$ and $k = 1, 2$, the above adjustments will be applied again for all the nodes, etc.

(c) We employ periodic boundary conditions during the procedure so as to make sure that the nodes continue to be in the physical space for all the course of time without being departed.

As hinted above, nodes will interact based on the concept of generation of random geometric graphs and hence they will communicate with only those that belong to a specified region (subregion) created for that particular node. For this, inside the physical space in which the nodes are moving, smaller square-shaped regions (calling them *vision size*) are assigned to every node. Here, we are considering square shaped vision sizes (analogous to the considered square-shaped lattice) in the direction of the motion of the nodes which is simple to understand and fits well with our platform of the node movement. It could have been chosen in other shapes like that of circular or cone shaped vision sizes as assumed in [69–71]. But what mostly matters is the area (volume) of the vision sizes. Keeping the area (volume) constant, the angle can have impacts that has not been dealt with in this work. Even, the random walk can be designed over lattice having different shapes, e.g., random walks in cone [72]. But without loss of generality, we here confine ourselves to the case of square-shaped vision sizes for each node within a square lattice.

So, whenever a node moves to its right (say) [cf. Eq. (1)] then a square-shaped vision size of area ϕ^2 is created to its right. Then the node will interact only with those nodes which lie in the vision size. Similarly, if a node is moving towards front [cf. Eq. (2)], then a square-shaped vision size of area ϕ^2 is created in that direction. As a matter of fact, the vision size for a particular node will be created in a direction along which the node moves, thus generating a random geometric graph [73,74], one of the most important and simple models of spatial networks [64]. For a better understanding, a simple graphical view of moving nodes in a single layer and creation of vision sizes at a particular instant of time is presented in Fig. 1(b).

Throughout the article, our main emphasis will be to unravel the prominence in the results obtained through the incorporation of mobility in the nodes of the network. For the sake of simplicity, we have considered $\phi_1 = \phi_2 = \phi$ and $u_1 = u_2 = u$. Hence, we will be mainly concentrating on the impacts of the parameters ϕ and u involved in the movement of the nodes. But the frequency of the network switching (node movement) has been considered as the maximum possible here, as at each integration time step the nodes move and the network connectivity gets reshaped. However, the following results have been well verified with lower frequencies in the movement (not shown here) that produce qualitatively similar results.

III. MULTIPLEX NETWORK OF MOBILE OSCILLATORS

We consider a bilayer multiplex network with N mobile nodes in each layer performing a 2D-lattice random walk. Each node i ($i = 1, 2, \ldots, N$) with position coordinate (ξ_i^k, η_i^k) [cf. Eq. (1)] is carrying a dynamical system whose

evolution is described by $\dot{X}_{k,i} = F(X_{k,i})$, where $X_{k,i}$ is an m-dimensional vector of dynamical variables of the ith oscillator and $F(X_{k,i})$ is a vector field characterizing the dynamical units, for the kth layer. The dynamical network is then given by the following set of equations:

$$\begin{aligned}\dot{X}_{1,i} &= F(X_{1,i}) - k_1 \sum_{j=1}^{N} g_{ij}^{1}(t) E_1(X_{1,j}) \\ &\quad + \epsilon[H(X_{2,i}) - H(X_{1,i})], \\ \dot{X}_{2,i} &= F(X_{2,i}) - k_2 \sum_{j=1}^{N} g_{ij}^{2}(t) E_2(X_{2,j}) \\ &\quad + \epsilon[H(X_{1,i}) - H(X_{2,i})], \end{aligned} \tag{2}$$

where k_1, k_2 are the intralayer interaction strengths among the random walkers in layer-1 and layer-2, respectively, while ϵ stands for the interlayer coupling strength. Here $G_1(t) = [g_{ij}^{1}(t)]_{N\times N}$ and $G_2(t) = [g_{ij}^{2}(t)]_{N\times N}$ are the time-varying zero-row sum Laplacian matrices of order N governing the connectivities in the layers at time t. Particularly, $g_{ij}^{k}(t) = -1$ if the jth oscillator lies in the vision size of the ith oscillator and otherwise is zero, with $k = 1, 2$. $E_k : \mathbb{R}^m \to \mathbb{R}^m$ and $H : \mathbb{R}^m \to \mathbb{R}^m$, respectively, correspond to the intralayer and interlayer output vectorial functions, $k = 1, 2$.

IV. RESULTS

Here we are concerned with a bilayer network where the layer nodes follow the dynamics of well known Rössler oscillators [75] with $F(X_{k,i})$ in the following form:

$$F(X_{k,i}) = \begin{pmatrix} -y_{k,i} - z_{k,i} \\ x_{k,i} + a y_{k,i} \\ b + z_{k,i}(x_{k,i} - c) \end{pmatrix}, \tag{3}$$

where $a = 0.2$, $b = 0.2$, $c = 5.7$ has been considered so as to keep the oscillators in a chaotic regime. Without loss of generality, we consider both intralayer and interlayer coupling functions to be linear diffusive through the variable y, i.e., $E_k(X_k) = (0, y_k, 0)'$ and $H(X_k) = (0, y_k, 0)'$ where $(\cdot)'$ denotes the transpose of a matrix, with $k = 1, 2$. Also, we fixed the parameters $P = Q = 300$, $N = 100$ throughout this paper and chose random initial conditions from the phase space volume $[-15, 15] \times [-15, 15] \times [0, 35]$ for the dynamical variables for numerical simulations [76].

A. Numerical results

First of all, we define the interlayer and intralayer synchronization errors, respectively, as follows:

$$E_1 = \lim_{T\to\infty} \frac{1}{T} \int_0^T \sum_{i=1}^{N} \frac{\|\delta W_i(t)\|}{N} dt \tag{4}$$

and $E_2 = (\mathbf{e_1} + \mathbf{e_2})/2$, with

$$\mathbf{e_k} = \lim_{T\to\infty} \frac{1}{T} \int_0^T \sum_{i,j=1(i\neq j)}^{N} \frac{\|X_{k,i}(t) - X_{k,j}(t)\|}{N(N-1)} dt; \quad k = 1, 2, \tag{5}$$

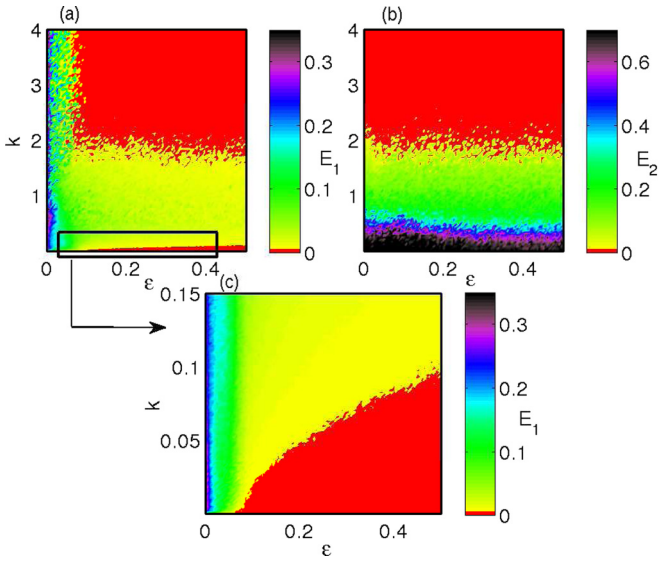

FIG. 2. (a) Interlayer synchronization error E_1 and (b) intralayer synchronization error E_2 in the k-ϵ parameter plane. A magnified version of a specified region in (a) is shown in (c).

where $\delta W_i(t) = X_{1,i}(t) - X_{2,i}(t)$ is the variable describing state difference between the ith replica nodes and $\|\cdot\|$ is the Euclidean norm. Basically, E_1 defines a long time [77] averaged difference between the replica nodes' dynamics of the two layers varying in the range [0, 0.35], the zero value [78] of which signifies interlayer synchronization. It corresponds to the situation in which each node in one of the layers is synchronized with its replica in the other layer, irrespective of whether or not it is in synchrony with the other dynamical units of that particular layer. However, E_2 is the sum of the intralayer errors that varies here in the range [0, 0.70], whose zero value actually correspond to the state of intralayer synchronization, whereby both layers are individually synchronized.

Let us now start by looking at the inter- and intralayer synchronization errors E_1 and E_2 with respect to simultaneous variation in the interlayer interaction strength ϵ and strength of intralayer coupling $k = k_1 = k_2$, plotted in Fig. 2 obtained through numerical simulations (averaged over 20 realizations) [77]. Here we have kept fixed the values of the vision range $\phi = 10$ and the step size $u = 6$. Figure 2(a) shows that as long as both k and ϵ are small enough, there is no sign of any kind of synchrony in the network. But, whenever ϵ crosses the value $\epsilon \simeq 0.10$ with k being small below $k \simeq 0.15$, the network experiences interlayer synchronization satisfying $E_1 \simeq 0$ represented by red color in the figure. However, as k increases, this occurrence of complete interlayer synchrony is getting hindered by intralayer interactions. This observation remains true until $k \simeq 2.0$ above which the perfect interlayer synchrony is witnessed again which persists further. In contrast to this, according to Fig. 2(b), intralayer synchrony characterized by $E_2 \simeq 0$ appears only when $k \gtrsim 2.0$ and remains for any higher k. This readily implies that in the region with small $k \lesssim 0.15$ reflecting interlayer synchrony (discussed above) there is no intralayer synchrony, i.e., synchronization in the replicas may be present even if both layers individually

possess asynchrony. But, in the region with $k \gtrsim 2.0$ and $\epsilon \gtrsim 0.10$, both inter- and intralayer synchronizations appear simultaneously. For a better perception of these phenomena, a magnified version of the specified region of Fig. 2(a) is presented in Fig. 2(c) with $0 \leqslant \epsilon \leqslant 0.50$ and $0 \leqslant k \leqslant 0.15$. From this figure, the values of E_1 implying interlayer synchrony are now conspicuous. Thus, for a fixed ϵ that exceeds 0.10, transitions from complete interlayer synchrony to disorder and to perfect interlayer synchrony again can be realized in the network with a variation in the intralayer coupling strength k and this needs further investigations. So, in the next subsection, we provide analytical results obtained through linear stability analysis to check whether they validate our numerical results.

B. Linear stability analysis

We proceed through the master stability function (MSF) approach to study the emergence and stability of interlayer synchronization. For this, let $\delta W_i = X_{1,i} - X_{2,i}$ be a small perturbation in the dynamics of the ith nodes of the two layers from the interlayer synchronization manifold $X_{1,i} = X_{2,i}$, for $i = 1, 2, \ldots, N$. This yield the linearized equation near this manifold (expanding up to the first order) as follows:

$$\delta \dot{W}_i = [JF(\tilde{X}_i) - 2\epsilon JH(\tilde{X}_i)]\delta W_i - k\sum_{j=1}^{N} g_{ij}^2 JE_2(\tilde{X}_j)\delta W_j + k\sum_{j=1}^{N} \Delta g_{ij} E_2(\tilde{X}_j), \quad (6)$$

with $\Delta g_{ij} = g_{ij}^1 - g_{ij}^2$ as the difference between the two Laplacians, J stands for the Jacobian, and $\tilde{X}_i$ being the state variable corresponding to the isolated ith node following:

$$\dot{\tilde{X}}_i = F(\tilde{X}_i) - k\sum_{j=1}^{N} g_{ij}^1 E_1(\tilde{X}_j). \quad (7)$$

Here the final term on the right-hand side of Eq. (6) drives the system away from the interlayer synchronization manifold whenever the interaction topologies of the two layers differ significantly. However, it is expected that when the difference between the two topologies is very small, the MSF approach is applicable [54]. As clarified earlier, the mobility parameters together with the interaction strengths of the individual layers have been taken the same in the present article so that the two layers remain *statistically equivalent* [79]. Actually, the two layers not only maintains similar degree distributions, there can be connection similarity (low distance) as well [80,81]. This helps in making the difference Δg_{ij} appearing in the last term of Eq. (6) small so that the negativity of the maximum Lyapunov exponent (MLE) Λ_1 from Eqs. (6) and (7) corresponds to stable interlayer synchrony as the perturbation transverse to the manifold vanishes.

However, for intralayer synchrony, let the manifolds of the two layers be $S_1(t) = X_{1,i}(t)$ and $S_2(t) = X_{2,i}(t)$, for $i = 1, 2, \ldots, N$ where $\delta X_{1,i}(t)$ and $\delta X_{2,i}(t)$ are the deviations from the respective manifolds implying $X_{1,i}(t) = S_1(t) + \delta X_{1,i}(t)$ and $X_{2,i}(t) = S_2(t) + \delta X_{2,i}(t)$. Then the perturbed linearized equations become

$$\delta \dot{X}_{1,i} = JF(S_1)\delta X_{1,i} - k\sum_{j=1}^{N} g_{ij}^1 JE_1(S_1)\delta X_{1,j} + \epsilon[JH(S_2)\delta X_{2,i} - JH(S_1)\delta X_{1,i}] \quad (8)$$

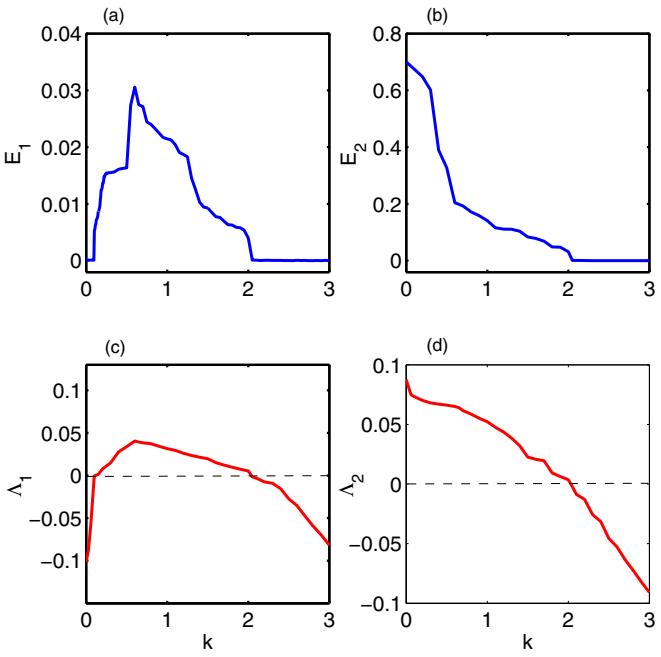

FIG. 3. (a) Interlayer and (b) intralayer synchronization errors E_1 and E_2, respectively; maximum Lyapunov exponents (c) Λ_1 and (d) Λ_2, respectively, for inter- and intralayer synchronization, all with respect to the parameter k where $\epsilon = 0.50$. The other parameters are $\phi = 10$ and $u = 6$.

and

$$\delta \dot{X}_{2,i} = JF(S_2)\delta X_{2,i} - k\sum_{j=1}^{N} g_{ij}^2 JE_2(S_2)\delta X_{2,j} + \epsilon[JH(S_1)\delta X_{1,i} - JH(S_2)\delta X_{2,i}], \quad (9)$$

with $(\tilde{X}_{1,i}, \tilde{X}_{2,i})$ as the state variables of the system

$$\dot{\tilde{X}}_{1,i} = F(\tilde{X}_{1,i}) + \epsilon[H(\tilde{X}_{2,i}) - H(\tilde{X}_{1,i})]$$
$$\dot{\tilde{X}}_{2,i} = F(\tilde{X}_{2,i}) + \epsilon[H(\tilde{X}_{1,i}) - H(\tilde{X}_{2,i})]. \quad (10)$$

Next solving the linearized systems Eqs. (8) and (9) along with the nonlinear Eq. (10), two maximum Lyapunov exponents transverse to the intralayer synchronization manifolds $S_1(t) = X_{1,i}(t)$ and $S_2(t) = X_{2,i}(t)$ are computed. Then the negativity of the maximum value (Λ_2) between these two MLE's characterizes the existence and stability of the intralayer synchronization as this situation reflects the occurrence of complete synchronization of the individual layers. In the following, we vary the intralayer coupling strength k (with fixed values of ϕ and u which do not appear explicitly in the MSF but they actually govern the Laplacians g_{ij}^k in the equations) and observe the variations in the errors as well as in Λ_1 and Λ_2.

Figures 3(a) and 3(b), respectively, show the inter- and intralayer synchronization errors E_1 and E_2 with respect to the intralayer coupling strength k, while the interlayer interaction strength is kept fixed at $\epsilon = 0.50$. Initially, E_1 retains its value to $E_1 \simeq 0$ until $k \simeq 0.10$. Then E_1 starts varying and remains nonzero in the range $0.10 \leqslant k \leqslant 2.05$ signifying the state of out-of synchrony. However, for $k > 2.05$, E_1 becomes zero

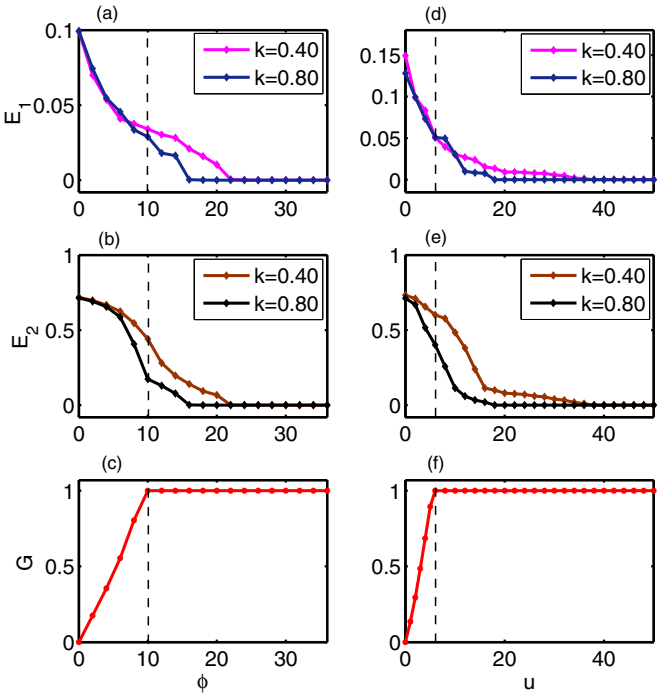

FIG. 4. (a, d) Interlayer and (b, e) intralayer synchronization errors E_1 and E_2 together with (c, f) the normalized size G of the giant connected component against ϕ (the left panel) with $u = 6$ fixed and against u (the right panel) having $\phi = 10$ fixed. Here $\epsilon = 0.20$. The vertical lines in the two panels correspond to the values $\phi = 10$ and $u = 6$ which are used in Fig. 2.

again implying the reoccurrence of interlayer synchronization. On the contrary, starting with nonzero values, E_2 turns into zero only when k passes the value $k = 2.05$ and remains zero for higher k. This whole scenario is then verified with the values of Λ_1 and Λ_2 calculated following the procedure described above. As in Fig. 3(c), Λ_1 remains negative as long as $k \leqslant 0.10$, but it starts increasing beyond zero as k increases and Λ_1 stays positive for $0.10 \leqslant k \leqslant 2.05$. Thereafter, Λ_1 is observed to be negative confirming the emergence and stability of interlayer synchrony. Moreover, the change in Λ_2 is also depicted in Fig. 3(d) where Λ_2 initializing from positive values, it turns to be negative whenever k crosses the value $k = 2.05$ that validates the appearance of intralayer synchronization.

C. Impacts of vision range and step size

So far, the results discussed are mainly due to the variation in the two types of interaction strengths k and ϵ in which the influences of either the vision range ϕ or the step size u has not been tested yet. But as we are dealing with a special network formalism of mobile nodes, the consequences of variation in ϕ and u deserve attentive study. The errors E_1 and E_2 are plotted against increasing ϕ for two different $k = 0.40$ and $k = 0.80$, while keeping all the other network parameters fixed at $\epsilon = 0.20$ and $u = 6$, in Figs. 4(a) and 4(b). As can be seen in Fig. 4(a) for $k = 0.40$, there is no sign of interlayer synchrony (as, E_1 is not near zero) till $\phi < 22$. But quite interestingly even though ϕ actually regulates the intralayer movements, when ϕ increases beyond this value the network experiences interlayer synchronization. For higher intralayer coupling strength $k = 0.80$, again from nonzero values, E_1 turns out to be zero for $\phi \geqslant 16$. A similar transition has been realized in E_2 for increasing ϕ. With both $k = 0.40$ and $k = 0.80$, E_2 decreases quite rapidly due to the increment in ϕ and eventually becomes zero respectively at $\phi = 22$ and $\phi = 16$ meaning the emergence of intralayer synchrony.

Next we identify the normalized (relative) size G (obtained through dividing the actual size by the total size N of the network) of the giant connected component [82,83], while taking the multiplex network as an ordinary network by averaging over 500 time units and over 10 realizations. We plot G as a function of ϕ in Fig. 4(c) that explains how G starts increasing rapidly with ϕ and eventually approaches unity for $\phi \geqslant 10$, so that the network gets settled into a single component. This percolation is followed by the emergence of synchronizations as depicted in Figs. 4(a) and 4(b). Of course, it depends on the value of k, the higher the value of k, the lower the ϕ is needed.

We then want to go for studying the effect of the step size u on these two types of synchronization phenomena. For this, we have chosen $k = 0.40$ and $k = 0.80$ with $\epsilon = 0.20$ as above and kept $\phi = 10$ fixed. Figure 4(d) depicts the values of E_1 with respect to variation in the step size $u \geqslant 0$. From this, one is able to see that E_1 goes to zero at $u = 38$ whenever $k = 0.40$ and while $k = 0.80$ interlayer synchrony appears for $u = 18$. This means changing only the step size of the nodes in the layers, one can achieve interlayer synchronization. Besides, we have also plotted E_2 versus u for $k = 0.40$ and 0.80 in Fig. 4(e) where again a similar sort of transition has been observed. The relative size G of the giant connected component with respect to u is plotted in Fig. 4(f) in which increasing G reaches to the unit value for $u \geqslant 6$ after which synchronization occurs.

For an outright visualization of this influence of the mobility parameters ϕ and u on the synchronized states, we further went to plot the errors E_1 and E_2 in the k-ϵ coupling parameter plane. The errors E_1 and E_2 are respectively shown in Figs. 5(a) and 5(b) in the $k - \epsilon$ plane for $\phi = 20$ and $u = 10$ fixed. Similar scenarios can be realized here as found in Figs. 2(a) and 2(b). For very small $k \leqslant 0.05$, increasing ϵ may induce interlayer synchrony, but higher $k \leqslant 0.45$ can disturb this as well. However this is not the case for intralayer synchronization. Above $k \simeq 0.45$ (which was $k \simeq 2.0$ for $\phi = 10$ and $u = 6$) both inter- and intralayer synchronization take place in the network. With higher $\phi = 30$ and $u = 15$, both synchronized states appear even earlier beyond $k \simeq 0.15$. This is how the intralayer mobility parameters ϕ and u help in not only forming intralayer ordering, but also they are quite effective in creating interlayer synchronized activities.

To have an additional view of the effect of alteration in the interlayer coupling strength ϵ on the intralayer synchronization, we plot the error E_2 in the k_1-k_2 plane (cf. Fig. 6). Here the two layers possess two different interaction strengths k_1 and k_2. We start with a small $\epsilon = 0.01$ in Fig. 6(a) where intralayer synchrony does not show up unless the coupling strengths satisfy $k_1 \gtrsim 2.0$ and $k_2 \gtrsim 2.0$. But with a higher $\epsilon = 0.05$, the region reflecting intralayer synchrony gets enlarged in the $k_1 - k_2$ plane, as can be seen from Fig. 6(b).

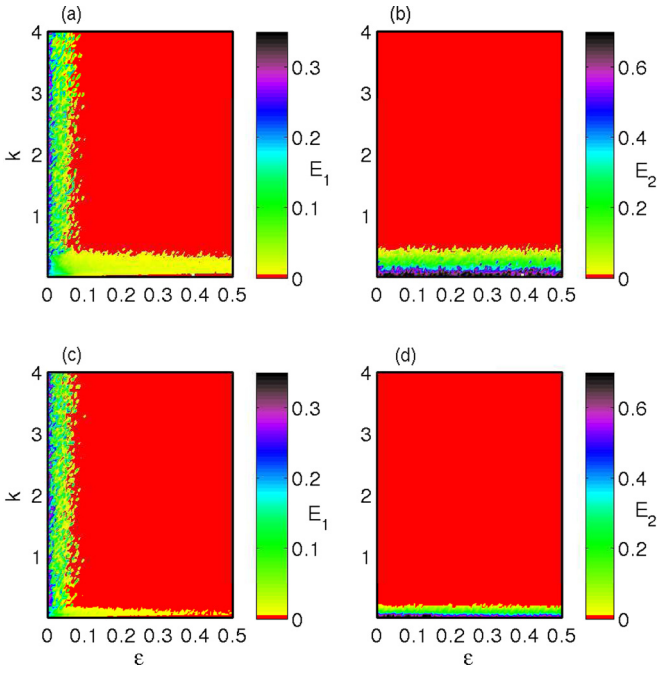

FIG. 5. (a), (c) Interlayer synchronization error E_1 and (b), (d) intralayer synchronization error E_2 for simultaneous variation of k and ϵ. Here $\phi = 20$, $u = 10$ for (a), (b) and $\phi = 30$, $u = 15$ for (c), (d).

With higher $\epsilon = 0.20$ and $\epsilon = 0.40$, the area of synchrony becomes even larger, as discernible from Figs. 6(c) and 6(d). This establishes the ability of interlayer interaction strength in enhancing intralayer synchronization as well.

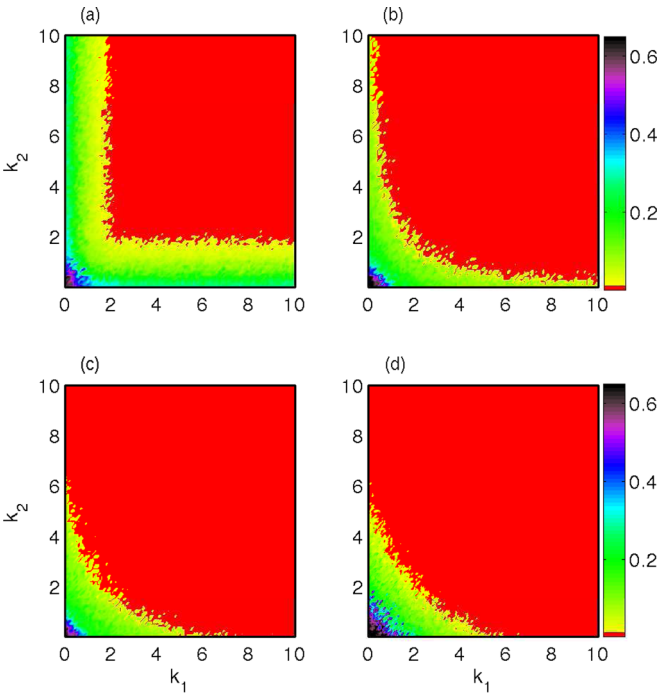

FIG. 6. Intralayer synchronization error E_2 (in color bar) in the k_1-k_2 parameter plane with (a) $\epsilon = 0.01$, (b) $\epsilon = 0.05$, (c) $\epsilon = 0.20$, (d) $\epsilon = 0.40$. Other parameters are $\phi = 10$ and $u = 6$.

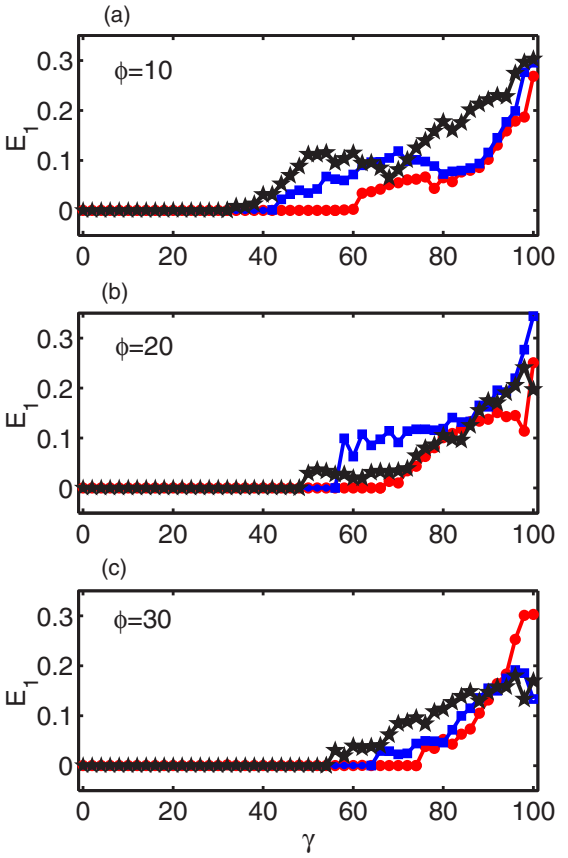

FIG. 7. Interlayer synchronization error E_1 as function of the number of demultiplexed nodes γ for three different values of $k = 3.0$, 10.0, and 20.0 in black, blue, and red, respectively, with (a) $\phi = 10$, (b) $\phi = 20$, and (c) $\phi = 30$. Here $u = 6$.

V. TOPOLOGICAL PERTURBATION

A. Influence of demultiplexing

For further understanding about the development of synchronization on such an important framework of the network, now we will be dealing with the issue of robustness of synchronization, particularly, interlayer synchrony (as this is one of the most nontrivial behavior arising under the multiplex formalism) against progressive random demultiplexing (as a form of perturbation in the links). The continuous demultiplexing is done through sequentially removing (randomly chosen) interlayer links one by one until the two layers become entirely isolated [53].

Figure 7(a) shows the interlayer synchronization error E_1 against the number of demultiplexed nodes γ starting with 0 to $N(= 100)$. Here, fixed interlayer coupling strength $\epsilon = 0.20$ and different values of the intralayer interaction strength k are dealt with, for $\phi = 10$ and $u = 6$. As we begin with $k = 3.0$, one can see that E_1 starting from zero, suddenly becomes nonzero whenever $\gamma = 32$. This essentially means that the interlayer synchrony is unable to survive for demultiplexing of $\gamma = 32$ replica nodes, but continues to be present even when 31 pairs of nodes are demultiplexed. This is because as long as there are possibilities of (indirect) communication between the demultiplexed pairs of nodes, interlayer synchrony will

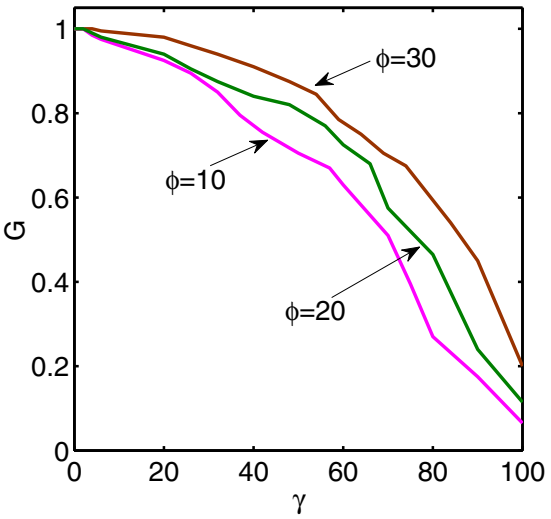

FIG. 8. Normalized size G of the giant connected component with respect to the number of demultiplexed nodes γ for three different values of the vision range $\phi = 10$, $\phi = 20$, and $\phi = 30$.

be there depending on the strength of coupling the nodes are tied with. This can be further illustrated by choosing higher values of k. Interestingly, as the intralayer coupling strength k is taken larger than that in the previous case, namely with $k = 10.0$, the synchrony persists until $\gamma = 42$ (the curve in blue). This shows what a crucial role the intralayer connectivity in terms of k, is playing here. Even higher $k = 20.0$ makes this critical value of γ as $\gamma = 57$ (the curve in red) that maintains interlayer synchrony keeping $E_1 = 0$.

Next we investigate the effect of one of the mobility parameter, namely the vision range ϕ on this demultiplexing and consequently the persistence of the interlayer synchrony. In Fig. 7(b), we plot E_1 with respect to γ for $\phi = 20$, while keeping all the other parameters fixed as above. Remarkably, with this ϕ and $k = 3.0$, E_1 remains zero until the number of demultiplexed nodes exceeds $\gamma = 48$ which was previously $\gamma = 32$ when $\phi = 10$ was taken. Thus for larger ϕ, interlayer synchrony persists even when the interlayer interaction has been perturbed between a large number of replica nodes. Whenever $k = 10.0$ and $k = 20.0$ is considered, synchrony survives up to $\gamma = 56$ and $\gamma = 66$, respectively, which were $\gamma = 42$ and $\gamma = 57$ earlier. These figures demonstrate that as long as the nodes in each layer get the opportunity of more interactions with other nodes through the generation of larger vision ranges by increasing the value of ϕ, they can rescue the interlayer synchrony of the network. This scenario is further validated taking $\phi = 30$ into account in Fig. 7(c). Here, the critical values of γ that retain synchrony, increase over and above and become $\gamma = 54$, 64, and 74 for $k = 3.0$, 10.0, and 20.0, respectively.

Figure 8 depicts the evolution of the giant connected component against the progressive demultiplexing in the network and G is plotted with respect to γ for the same set of values of $\phi \in \{10, 20, 30\}$ as in Fig. 7. Whenever $\phi = 10$, starting with unit value for $\gamma = 0$, it decreases monotonically with increasing γ depending on which after certain values (of course, it depends on the coupling strength) of γ [84], the network loses interlayer synchrony. A similar trend in G for other ϕ's is

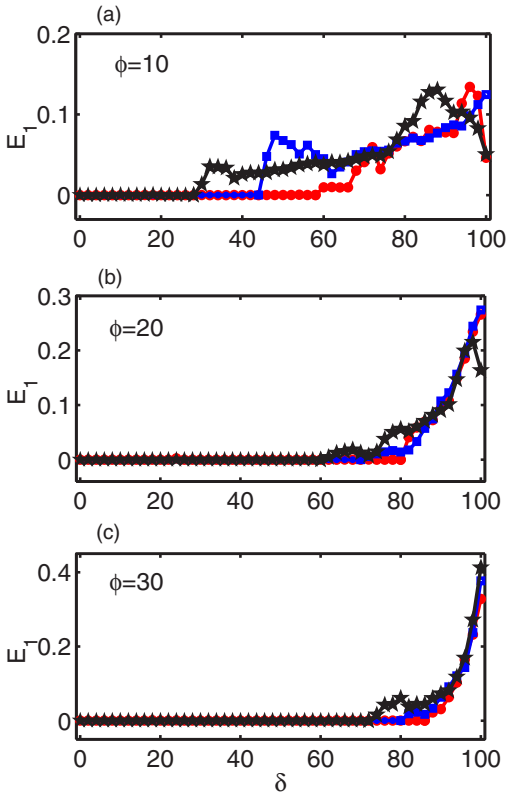

FIG. 9. Interlayer synchronization error E_1 with respect to the number of static nodes δ with three different values of $k = 3.0$, 6.0 and 10.0 in black, blue and red respectively, for (a) $\phi = 10$, (b) $\phi = 20$, and (c) $\phi = 30$. Here $u = 6$ is fixed.

observed but more importantly as we deal with higher vision ranges $\phi = 20$ and $\phi = 30$, the values of G are essentially higher (or equal) throughout the whole range of $\gamma \in [0, N]$, respectively, varying in the ranges [0.12, 1.0] and [0.2, 1.0] that helps in sustaining synchrony even when a large number of node pairs are demultiplexed [cf. Figs. 7(b) and 7(c)]. These results indicate that the interlayer synchronization can survive against significant demultiplexing if it is compensated by a larger vision range of the nodes that governs intralayer mobility.

B. Effect of static nodes

Next we move on to analyze the survivability of interlayer synchrony against successively created static replica nodes (randomly chosen a pair of replica nodes and prescribed $u = 0$) in each layer (as a form of disturbance in the nodes). This study is highly reasonable in many ways as some nodes (e.g., in ecological, social networks) may, indeed, undergo immobility quite naturally or as a result of environmental influence. We will also examine whether mobility parameters (like ϕ) have any decisive influence in enhancing the persistence of interlayer synchronization.

In Fig. 9(a), E_1 is plotted with respect to the number of static nodes $\delta \in [0, N]$ ($\delta = 0$ interpreting all nodes are moving, whereas $\delta = N$ means that all the nodes are static in the 2D space for the entire course of time) where $\epsilon = 0.20$, $\phi = 10$ and $u = 6$ are kept fixed. Whenever $k = 3.0$, E_1 turns

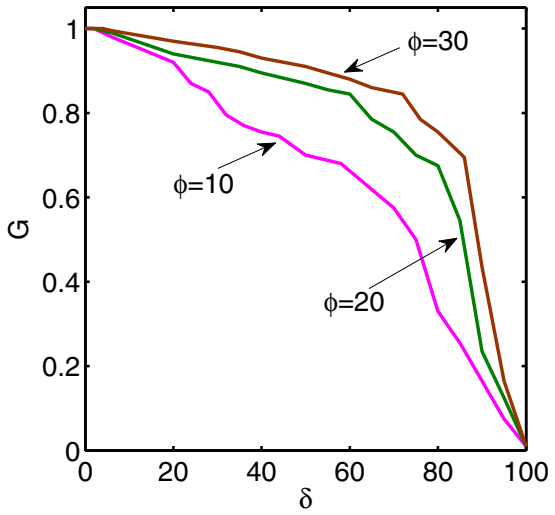

FIG. 10. Normalized size G of the giant connected component as function of the number of static nodes δ for three different values of the vision range $\phi = 10$, $\phi = 20$, and $\phi = 30$.

nonzero if $\delta = 28$ nodes in each layer become static (i.e., $u = 0$ for those particular nodes). Until $\delta = 28$, E_1 remains to be zero. This essentially means that the movement in the rest of the 72 nodes in each layer is sufficient to maintain interlayer synchronization in the network. Higher $k = 6.0$ and $k = 10.0$ helps the network to sustain interlayer synchrony even up to $\delta = 44$ and $\delta = 58$ respectively. So by increasing the intralayer interaction strength k, persistence of interlayer synchronization against static replica nodes can be enhanced.

As far as the influence of ϕ on this sort of transition is concerned, we assume the vision range ϕ to be $\phi = 20$ in Fig. 9(b). As seen, this ϕ has an amazing impact on the resilience of the interlayer synchrony, as the synchrony can still be present even when $\delta = 60$ nodes lose the ability to move any more, for $k = 3.0$. With higher $k = 6.0$ and 10.0, this ϕ helps the network in experiencing interlayer synchrony until $\delta = 70$ and 80 respectively. Figure 9(c) depicts the enhancement in the sustainability of synchrony in the network with $\phi = 30.0$. In this case, E_1 remains zero implying the persistence of interlayer synchrony up to $\delta = 72$, 80, and 86 for $k = 3.0$, 6.0, and 10.0, respectively.

The variations in G as a function of δ are figured out in Fig. 10 for these three values of ϕ. For $\phi = 10$, similar to the case of demultiplexing, starting with unity for $\delta = 0$, G decreases for increasing δ and finally reaches to $G = 0.01$ for $\delta = 100$, which is the least possible value of G attained when all the nodes become static having no intralayer connections and we are left with only one-to-one interlayer interactions. With $\phi = 20$ and $\phi = 30$, the nodes get opportunities to have more neighbors which leads G to own higher values (in the same range [0.01, 1.0]) and the network to reflect higher extent of robustness. This signifies that if the vision range is high enough then even if a large number of nodes fails to move, the network is still able to realize interlayer synchrony.

Such an outcome on augmentation in resilience of synchronization can also be helpful in the study of controlling synchronization which is a very important issue in several fields (e.g., neuronal evolution [85,86] in which the multiplex formalism [87] is evident as well, and some technological [88,89] and ecological [90,91] perspectives) and has been a topic of discussion for decades.

In this context, we would also like to note that with a different framework of the network (time-static or space-static), it is mainly the interaction strength that governs the evolution of synchronization, but here our study reveals that even if the coupling strength is kept unaltered, the mobility parameters ϕ and u will do the rest of the job under consideration.

VI. DYNAMICAL PERTURBATION

The above two sections were mainly devoted to the study of robustness of interlayer synchrony against some legitimate structural (topological) perturbations and the ability of the network to withstand those failures owing to the disturbance in links and nodes respectively. But the aspect of dynamical perturbation that has high practical relevance, has not been addressed yet. So, in this subsection, we will go through the discussion of the recently proposed basin stability analysis [92–96] based on the idea of targeted attacks to specific nodes of the network, termed as "single-node basin stability (SNBS)" [96]. This scheme of SNBS contributes in understanding the probability of the system to return to its desired stable state after a blow to that particular node through nonlocal arbitrary dynamical perturbations [97–100].

The procedure for calculating SNBS is as follows:

(i) Obtain the synchronization manifold $S(t) = (X_1, X_2, \ldots, X_N)$.

(ii) Choose M different points that sufficiently move through all parts of the attractor corresponding to the manifold $S(t)$.

(iii) Each time initializing the system from a single $m(m = 1, 2, \ldots, M)$, one needs to dynamically perturb the ith oscillator by uniformly picking I random initial conditions from the phase space of the networked system.

(iv) Among these I initial conditions, count those J initial conditions that reach the synchronized state. Then the SNBS of the ith node starting from the mth point on the attractor is defined as

$$\mathrm{BS}(i, m) = \frac{J}{I}, \tag{11}$$

(v) Averaging over total M-points on the manifold $S(t)$, the mean SNBS can be found as

$$\langle \mathrm{BS}(i) \rangle = \frac{1}{M} \sum_{m=1}^{M} \mathrm{BS}(i, m); \quad (i = 1, 2, \ldots, N). \tag{12}$$

Let us now have a look at the estimated values of $\langle \mathrm{BS}(i) \rangle$ of all the pairs of replica nodes $(i = 1, 2, \ldots, N)$, where for the computation, we have chosen $I = 1000$ random initial conditions from the phase space volume $[-15, 15] \times [-15, 15] \times [0, 35]$ of the individual dynamical units. $M = 10$ points on the interlayer synchronization manifold $S(t)$ have been considered.

So far, we have observed that whenever $k = 3.0$, $\epsilon = 0.20$ with $\phi = 10$ and $u = 6$, interlayer synchrony has appeared (cf. numerical and linear stability analysis) which is valid as long as the initial conditions are taken sufficiently close to the synchronization manifold. Figure 11 shows $\langle \mathrm{BS}(i) \rangle$ of

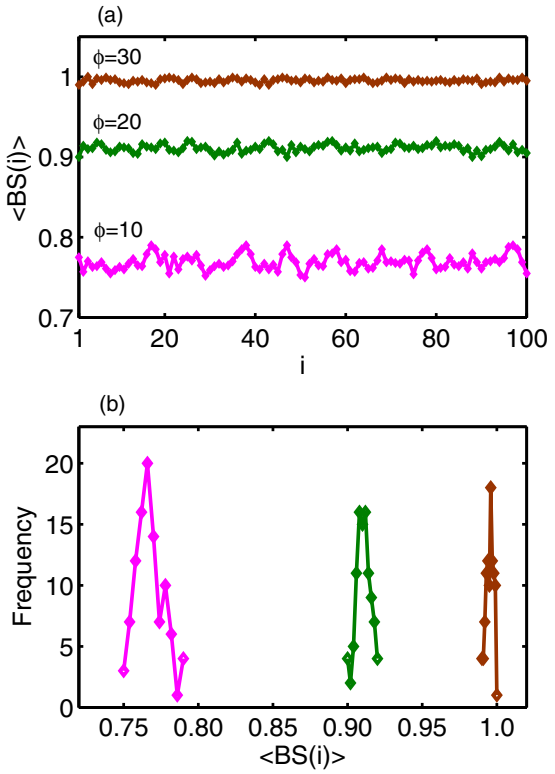

FIG. 11. Single-node basin stability $\langle \mathrm{BS}(i) \rangle$ of the interlayer synchronization for all the ith pairs of nodes: (a) $\phi = 10$ (magenta), $\phi = 20$ (deep green), and $\phi = 30$ (brown). The corresponding frequencies of $\langle \mathrm{BS}(i) \rangle$ are shown in (b). Other parameters are $k = 3.0$, $\epsilon = 0.20$, and $u = 6$.

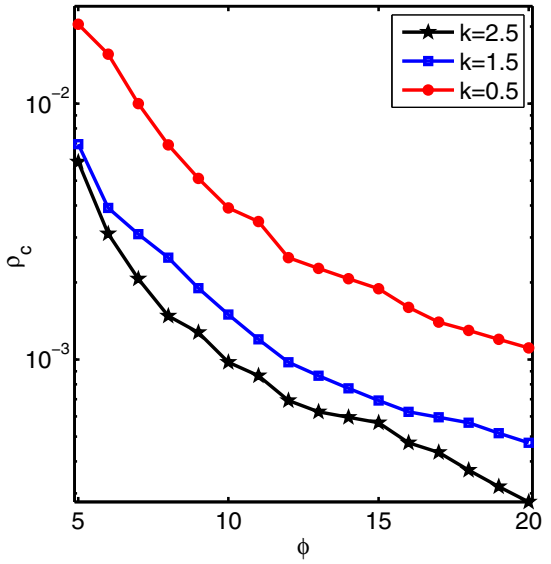

FIG. 12. The critical density ρ_c for the emergence of interlayer synchrony as a function of the vision range ϕ, for different values of k. The other parameters are fixed as $N = 100$, $\epsilon = 0.20$, and $u = 6$.

the replica nodes when all the replica nodes are dynamically disturbed from the interlayer synchronization state following the above defined mechanism. As in Fig. 11(a), the values of $\langle \mathrm{BS}(i) \rangle$ for all the $N = 100$ pairs of nodes (in magenta) are close to each other remaining in the range $[0.75, 0.79]$. As we noticed in the cases of topological perturbations (cf. Secs. V A and V B), here again due to an increase in the value of the intralayer mobility parameter (namely ϕ), the network experiences a notable development in the values of $\langle \mathrm{BS}(i) \rangle$ $(i = 1, 2, \ldots, N)$. This time, they lie in the range $[0.90, 0.92]$ (in deep green), as plotted for $\phi = 20$. For further raise in ϕ to $\phi = 30$, almost all the initial states eventually lead to the synchronized state, no matter which pairs of nodes are perturbed, with $\langle \mathrm{BS}(i) \rangle \in [0.99, 1.0]$ $(i = 1, 2, \ldots, N)$ (cf. the curve in brown). The corresponding frequencies of $\langle \mathrm{BS}(i) \rangle$ for all these three values of $\phi \in \{10, 20, 30\}$, are shown in Fig. 11(b). It is clear that $\langle \mathrm{BS}(i) \rangle$ increases monotonically with ϕ, while its dispersion has the opposite trend.

Thus, a sufficient vision range can substantiate an optimal response to perturbations on the nodes. This shows that not only the effects of topological fluctuations but the impacts of dynamical perturbations can also be recompensed through variation in mobility parameters of the network.

VII. CONCLUSIONS

We have demonstrated here the emergence of one of the most important collective behaviors in ensemble of oscillators, i.e., synchronization, in a multiplex dynamical network of mobile nodes. We have considered a two-layer network in which one-to-one correspondence between the replica nodes are preserved, in general. Chaotic dynamics arising from the Rössler system is used to cast the nodes of each layer in the network. The nodes in each layer are moving while performing a two-dimensional lattice random walk and regulate their movement after every time iteration. According to the network model presented, there are two coupling parameters, namely, the inter- and intralayer interaction strengths ϵ and k together with the mobility parameters: vision range ϕ and the step size u. Starting with the discussion of variation in k and ϵ, we have thoroughly investigated the alluring impacts of the intralayer mobility parameters ϕ and u in favoring not only the intralayer synchronization but also the interlayer synchrony. Apart from the numerical experiments, necessary conditions for the existence and stability of inter- and intralayer synchrony following master stability function approach has also been provided. For an outright understanding of the survivability of interlayer synchrony, we further applied structural perturbations in the form of progressive demultiplexing (link-based attack) and sequentially created static nodes (site-based attack). The outcomes suggest that an increment in the intralayer mobility parameter ϕ can immensely enhance and resurrect interlayer synchrony in the network from the disordered state. We have also illustrated the development of the giant connected component to explain these scenarios of synchronization while discussing the issues related to the mobility parameters. Besides this, dynamical perturbation while probing the notion of newly proposed single-node basin stability has also been implemented. Here again such consequence of ϕ in reviving interlayer synchrony particularly based on volumes of basin of attraction, is witnessed.

We hope that our findings open up new frontiers in the theory and application of synchronization from various

aspects, in particular for situations of individuals' mobility induced complexities.

ACKNOWLEDGMENTS

The authors are grateful to the anonymous referees for their very useful and constructive comments that helped in considerably improving the manuscript. D.G. was supported by the Department of Science and Technology, Government of India (Project No. EMR/2016/001039).

APPENDIX: EFFECT OF LATTICE SIZE

To demonstrate the effect of lattice size $L(= P = Q)$ on the appearance of synchrony, we first define the density ρ of the nodes in the lattice as $\rho = \frac{N}{L^2} = \frac{N}{PQ}$. Then keeping the value of N fixed at $N = 100$ and varying L, we find the critical value of this density ρ_c required to achieve interlayer synchronization. Next we plot these ρ_c with respect to increasing vision range ϕ in Fig. 12, for a variety of the values of intralayer coupling strength k. Looking at the profile of ρ_c for $k = 0.5$, it is cognizable that the more the ϕ, the less density is needed for synchrony; i.e., whenever ϕ increases, synchrony can be acquired even for larger lattice size L. For $k = 1.5$, this scenario remains valid but lesser ρ_c is required for the origination of synchrony. With higher $k = 2.5$, even lesser ρ_c appears to be sufficient for inducing synchronization. So, it can be concluded that even when lattice size is high, choice of adequate vision range can bring synchronization and even coupling strength can help in doing so as long as the network is connected.

[1] A. Pikovsky, M. Rosenblum, and J. Kurths, *Synchronization: A Universal Concept in Nonlinear Science* (Cambridge University Press, Cambridge, 2003).

[2] S. Boccaletti, J. Kurths, G. Osipov, D. L. Valladares, and C. S. Zhou, Phys. Rep. **366**, 1 (2002).

[3] S. H. Strogatz, *SYNC: the Emerging Science of Spontaneous Order* (Hyperion, New York, 2003).

[4] S. Majhi, B. K. Bera, D. Ghosh, and M. Perc, Phys. Life Rev. (2018), doi: 10.1016/j.plrev.2018.09.003.

[5] P. Holme and J. Saramäki, Phys. Rep. **519**, 97 (2012).

[6] M. L. Sachtjen, B. A. Carreras, and V. E. Lynch, Phys. Rev. E **61**, 4877 (2000).

[7] M. Valencia, J. Martinerie, S. Dupont, and M. Chavez, Phys. Rev. E **77**, 050905(R) (2008).

[8] J.-P. Onnela, J. Saramaki, J. Hyvonen, G. Szabo, D. Lazer, K. Kaski, J. Kertesz, and A. L. Barabasi, Proc. Natl. Acad. Sci. USA **104**, 7332 (2007).

[9] Y. Wu, C. Zhou, J. Xiao, J. Kurths, and H. J. Schellnhuber, Proc. Natl. Acad. Sci. USA **107**, 18803 (2010).

[10] J. L. Iribarren and E. Moro, Phys. Rev. Lett. **103**, 038702 (2009).

[11] R. Guimerà, L. Danon, A. Díaz-Guilera, F. Giralt, and A. Arenas, Phys. Rev. E **68**, 065103 (2003).

[12] R. Olfati-Saber, J. A. Fax, and R. M. Murray, Proc. IEEE **95**, 215 (2007).

[13] T. Gross, Carlos J. Dommar D'Lima, and B. Blasius, Phys. Rev. Lett. **96**, 208701 (2006).

[14] M. Frasca, A. Buscarino, A. Rizzo, L. Fortuna, and S. Boccaletti, Phys. Rev. E **74**, 036110 (2006).

[15] V. Kohar and S. Sinha, Chaos, Solitons Fractals **54**, 127 (2013).

[16] A. Buscarino, L. Fortuna, M. Frasca, and A. Rizzo, Chaos **16**, 015116 (2006).

[17] H. G. Tanner, A. Jadbabaie, and G. J. Pappas, in *Proceedings of the 42nd IEEE Conference on Decision and Control* (2003), pp. 2016–2021.

[18] J. Buhl, D. J. T. Sumpter, I. D. Couzin, J. J. Hale, E. Despland, E. R. Miller, and S. J. Simpson, Science **312**, 1402 (2006).

[19] K. Uriu, L. G. Morelli, and A. C. Oates, Semin. Cell Dev. Biol. **35**, 66 (2014).

[20] K. Uriu and L. G. Morelli, Biophys. J. **107**, 514 (2014).

[21] D. Tanaka, Phys. Rev. Lett. **99**, 134103 (2007).

[22] F. Sivrikaya and B. Yener, IEEE Network **18**, 45 (2004).

[23] K. Römer, in *Proceedings of the 2nd ACM International Symposium on Mobile ad hoc Networking & Computing* (ACM, NY, 2001), pp. 173–182.

[24] N. Fujiwara, J. Kurths, and A. Díaz-Guilera, Phys. Rev. E **83**, 025101(R) (2011).

[25] K. Uriu, S. Ares, A. C. Oates, and L. G. Morelli, Phys. Rev. E **87**, 032911 (2013).

[26] M. Frasca, A. Buscarino, A. Rizzo, L. Fortuna, and S. Boccaletti, Phys. Rev. Lett. **100**, 044102 (2008).

[27] S. Majhi and D. Ghosh, Chaos **27**, 053115 (2017); S. Rakshit, S. Majhi, B. K. Bera, S. Sinha, and D. Ghosh, Phys. Rev. E **96**, 062308 (2017); S. Majhi and D. Ghosh, Europhys. Lett. **118**, 40002 (2017).

[28] L. Prignano, O. Sagarra, and A. Díaz-Guilera, Phys. Rev. Lett. **110**, 114101 (2013).

[29] F. Peruani, E. M. Nicola, and L. G Morelli, New J. Phys. **12**, 093029 (2010).

[30] N. Fujiwara, J. Kurths, and A. Díaz-Guilera, Chaos **26**, 094824 (2016).

[31] B. Kim, Y. Do, and Y.-C. Lai, Phys. Rev. E **88**, 042818 (2013).

[32] D. Levis, I. Pagonabarraga, and A. Díaz-Guilera, Phys. Rev. X **7**, 011028 (2017).

[33] R. Großmann, F. Peruani, and M. Bär, Phys. Rev. E **93**, 040102(R) (2016).

[34] M. Szell, R. Lambiotte, and S. Thurner, Proc. Natl. Acad. Sci. USA **107**, 13636 (2010).

[35] B. M. Adhikari, A. Prasad, and M. Dhamala, Chaos **21**, 023116 (2011).

[36] A. Cardillo, M. Zanin, J. Gómez-Gardeñes, M. Romance, A. García del Amo, and S. Boccaletti, Eur. Phys. J. Spec. Top. **215**, 23 (2013).

[37] M. Kivelä, A. Arenas, M. Barthelemy, J. P. Gleeson, Y. Moreno, and M. A. Porter, J. Complex Netw. **2**, 203 (2014).

[38] S. Boccaletti, G. Bianconi, R. Criado, C. I. del Genio, J. Gómez-Gardeñes, M. Romance, I. Sendiña-Nadal, Z. Wang, and M. Zanin, Phys. Rep. **544**, 1 (2014).

[39] S. Gómez, A. Díaz-Guilera, J. Gómez-Gardeñes, C. J. Pérez-Vicente, Y. Moreno, and A. Arenas, Phys. Rev. Lett. **110**, 028701 (2013).

[40] M. De Domenico, A. Solé-Ribalta, E. Cozzo, M. Kivelä, Y. Moreno, M. A. Porter, S. Gómez, and A. Arenas, Phys. Rev. X **3**, 041022 (2013).

[41] V. Nicosia, G. Bianconi, V. Latora, and M. Barthelemy, Phys. Rev. Lett. **111**, 058701 (2013).

[42] S. V. Buldyrev, R. Parshani, G. Paul, H. E. Stanley, and S. Havlin, Nature **464**, 1025 (2010).

[43] J. Gao, S. V. Buldyrev, H. E. Stanley, and S. Havlin, Nat. Phys. **8**, 40 (2012).

[44] D. Helbing, Nature **497**, 51 (2013).

[45] B. Podobnik, A. Majdandzic, C. Curme, Z. Qiao, W.-X. Zhou, H. E. Stanley, and B. Li, Phys. Rev. E **89**, 042807 (2014).

[46] B. Podobnik, D. Horvatic, T. Lipic, M. Perc, J. M. Buldú, and H. E. Stanley, J. R. Soc. Interface **12**, 20150770 (2015).

[47] A. Cardillo, J. Gómez-Gardeñes, M. Zanin, M. Romance, D. Papo, F. del Pozo, and S. Boccaletti, Sci. Rep. **3**, 01344 (2013).

[48] C. Granell, S. Gómez, and A. Arenas, Phys. Rev. Lett. **111**, 128701 (2013).

[49] S.-W. Son, G. Bizhani, C. Christensen, P. Grassberger, and M. Paczuski, Europhys. Lett. **97**, 16006 (2012).

[50] X. Zhang, S. Boccaletti, S. Guan, and Z. Liu, Phys. Rev. Lett. **114**, 038701 (2015).

[51] V. H. P. Louzada, N. Araújo, J. S. Andrade, and H. J. Herrmann, Sci. Rep. **3**, 3289 (2013).

[52] S. Jalan and A. Singh, Europhys. Lett. **113**, 30002 (2016).

[53] R. Sevilla-Escoboza, I. Sendiña-Nadal, I. Leyva, R. Gutiérrez, J. M. Buldú, and S. Boccaletti, Chaos **26**, 065304 (2016).

[54] I. Leyva, R. Sevilla-Escoboza, I. Sendiña-Nadal, R. Gutiérrez, J. M. Buldú, and S. Boccaletti, Sci. Rep. **7**, 45475 (2017).

[55] L. V. Gambuzza, M. Frasca, and J. Gómez-Gardeñes, Europhys. Lett. **110**, 20010 (2015).

[56] S. Rakshit, B. K. Bera, and D. Ghosh, Phys. Rev. E **98**, 032305 (2018).

[57] C. I. del Genio, J. Gómez-Gardeñes, I. Bonamassa, and S. Boccaletti, Sci. Adv. **2**, e1601679 (2016).

[58] S. Majhi, M. Perc, and D. Ghosh, Sci. Rep. **6**, 39033 (2016).

[59] V. A. Maksimenko, V. V. Makarov, B. K. Bera, D. Ghosh, S. K. Dana, M. V. Goremyko, N. S. Frolov, A. A. Koronovskii, and A. E. Hramov, Phys. Rev. E **94**, 052205 (2016).

[60] S. Majhi, M. Perc, and D. Ghosh, Chaos **27**, 073109 (2017).

[61] R. Gallotti and M. Barthelemy, Sci. Data **2**, 140056 (2015).

[62] S. Pilosof, M. A. Porter, M. Pascual, and S. Kéfi, Nature Ecol. Evol. **1**, 0101 (2017).

[63] R. V. Solé and J. Bascompte, *Self-Organization in Complex Ecosystems* (Princeton University Press, Princeton, NJ, 2006).

[64] M. Barthélemy, Phys. Rep. **499**, 1 (2011).

[65] M. De Domenico, C. Granell, M. A. Porter, and A. Arenas, Nat. Phys. **12**, 901 (2016).

[66] M. Stella, C. S. Andreazzi, S. Selakovic, A. Goudarzi, and A. Antonioni, J. Complex Netw. **5**, 486 (2017).

[67] Y.-H. Eom, S. Boccaletti, and G. Caldarelli, Sci. Rep. **6**, 27111 (2016).

[68] P. Révész, *Random Walk in Random and Non-Random Environments* (World Scientific, Singapore, 2005).

[69] A. Beardo, L. Prignano, O. Sagarra, and A. Díaz-Guilera, Phys. Rev. E **96**, 062306 (2017).

[70] F. Perez-Diaz, R. Zillmer, and R. Groß, Phys. Rev. Appl. **7**, 054002 (2017).

[71] F. Perez-Diaz, R. Zillmer, and R. Groß, *Proceedings of the* 14th *International Conference on Autonomous Agents and Multiagent Systems* (2015), p. 279.

[72] D. Denisov and V. Wachtel, Ann. Probab. **43**, 992 (2015).

[73] J. Dall and M. Christensen, Phys. Rev. E **66**, 016121 (2002).

[74] M. Penrose, *Random Geometric Graphs* (Oxford University Press, Oxford, 2003).

[75] O. E. Rössler, Phys. Lett. A **57**, 397 (1976).

[76] We integrated the network Eq. (3) following fifth-order Runge-Kutta-Fehlberg algorithm with a time-step size of $h = 0.01$.

[77] For our computation, T is chosen to be 2×10^5 time units after an initial transient of 2×10^5 time units.

[78] In our simulations, the values of E_1 and E_2 less than 10^{-5}, respectively, correspond to inter- and intralayer synchronizations.

[79] The assumption of statistical equivalence between the Laplacians of the layers is justified here as the nodes move fast enough. In fact, they move and hence update their positions after each and every time iteration. But, in the cases of lower frequency in the node movements, this assumption may not be valid as there would be memory effects and hence the Laplacians may diverge.

[80] T.-C. Kao and M. A. Porter, J. Stat. Phys. **173**, 1286 (2018).

[81] In particular, if $A^1_{ij}(t)$ and $A^2_{ij}(t)$ are the adjacency matrices of the layers at time t, then the distance $D^{1,2}(t) \in [0, 1]$ between the layers at time t can be computed as $1 - S^{1,2}(t)$, $S^{1,2}(t)$ being the connection similarity $S^{1,2}(t) = \frac{1}{N}\sum_i S_i^{1,2}(t)$, with $S_i^{1,2}(t) = \frac{o_i^{1,2}(t)}{d_i^1(t)+d_i^2(t)-o_i^{1,2}(t)}$, where $d_i^k(t)$ is the degree of the ith node in the kth layer at time t and $o_i^{1,2}(t) = \sum_j A^1_{ij}(t)A^2_{ij}(t)$ counts the number of overlapping edges incident to ith node in layer-1 and layer-2. Along with the similar degree distributions in the layers, one can find small values of $D^{1,2}(t)$ as long as one deals with the same ϕ and u in the layers.

[82] V. Nicosia, J. Tang, M. Musolesi, G. Russo, C. Mascolo, and V. Latora, Chaos **22**, 023101 (2012).

[83] This giant connected component is computed for the underlying undirected network, which is usually known as the weakly connected component. The symmetry of the relation of synchronization and the possibility of synchrony through unidirectional coupling sufficiently allows one to calculate the weakly connected component in this context.

[84] To achieve only interlayer synchronization, the network does not necessarily possess unit value of G, smaller values of G may suffice as long as there are possibilities of (indirect) communication between the demultiplexed pairs of nodes.

[85] P. J. Uhlhaas and W. Singer, Neuron **52**, 155 (2006).

[86] L. Good, S. Sabesan, S. Marsh, K. Tsakalis, D. Treiman, and L. D. Iasemidis, Int. J. Neural Syst. **19**, 173 (2009).

[87] M. Vaiana and S. F. Muldoon, J. Nonlinear Sci. (2018), doi: 10.1007/s00332-017-9436-8.

[88] R. Cohen, K. Erez, D. ben-Avraham, and S. Havlin, Phys. Rev. Lett. **85**, 4626 (2000).

[89] L. Cuadra, S. Salcedo-Sanz, J. Ser, S. Jimenez-Fernandez, and Z. Geem, Energies **8**, 9211 (2015).

[90] M. D. Holland and A. Hastings, Nature (London) **456**, 792 (2008).
[91] E. Ranta, V. Kaitala, J. Lindstrom, and H. Linden, Proc. R. Soc. London B **262**, 113 (1995).
[92] P. J. Menck, J. Heitzig, N. Marwan, and J. Kurths, Nat. Phys. **9**, 89 (2013).
[93] S. Leng, W. Lin, and J. Kurths, Sci. Rep. **6**, 21449 (2016).
[94] S. Rakshit, B. K. Bera, S. Majhi, C. Hens, and D. Ghosh, Sci. Rep. **7**, 45909 (2017).
[95] S. Rakshit, B. K. Bera, M. Perc, and D. Ghosh, Sci. Rep. **7**, 2412 (2017).
[96] C. Mitra, A. Choudhary, S. Sinha, J. Kurths, and R. V. Donner, Phys. Rev. E **95**, 032317 (2017).
[97] A. E. Motter and Y.-C. Lai, Phys. Rev. E **66**, 065102 (2002).
[98] M. Pascual and J. A. Dunne, *Ecological Networks: Linking Structure to Dynamics in Food Webs* (Oxford University Press, Oxford, 2005).
[99] V. Kohar, P. Ji, A. Choudhary, S. Sinha, and J. Kurths, Phys. Rev. E **90**, 022812 (2014).
[100] C. Mitra, J. Kurths, and R. V. Donner, Sci. Rep. **5**, 16196 (2015).